Spiral Two-Phase Dendrites

Silvère Akamatsu,[1,*] Mikaël Perrut,[2] Sabine Bottin-Rousseau,[1] and Gabriel Faivre[1]
[1]*INSP, UPMC Univ. Paris 6, CNRS UMR 7588, 140 rue de Lourmel, 75015 Paris, France*
[2]*DMSM, ONERA, 29 Avenue de la Division Leclerc, 92322 Châtillon Cedex, France*
(Received 14 October 2009; published 5 February 2010)

We present real-time observations of a new growth pattern called a spiral two-phase dendrite, which we observed during univariant directional solidification of a ternary-eutectic alloy. Two different crystal phases grow from the apex of a parabolic finger, forming a spiral pattern that leaves behind in the solid a double helix microstructure. The parabola tip radius is nearly equal to the helix step. These lengths vary approximately as the reciprocal of the square root of the tip growth velocity. The direction of growth is not selected, but is initial-condition dependent.

DOI: 10.1103/PhysRevLett.104.056101 PACS numbers: 68.70.+w, 81.30.Fb

The solidification patterns (growth shapes and microstructures) of nonfaceted alloy crystals are an important subject for both material sciences [1] and the physics of systems out of equilibrium [2]. Their formation is primarily governed by a solute redistribution process, which involves solutal equilibration at the solid-liquid interface and solutal diffusion in the liquid [3]. Their global features depend on the number of components in the alloy, the number of coupled phases in the crystal, and the geometry of the solidification setup. We focus on solidification performed at a fixed rate V under a uniaxial thermal gradient (directional solidification). A single-phase crystal directionally solidified from a binary melt gives rise, typically, to dendritic patterns with spacings in the 100 μm range [4], whereas a two-phase crystal generates planar arrays of the two phases (eutectic patterns) with spacings in the 1 μm range [5]. Recently much interest has arisen in the solidification patterns of ternary-eutectic alloys [6,7]. In this Letter, we report on a novel ternary-eutectic solidification pattern called spiral two-phase dendrite (*sp* dendrite). The nature of this entity can be briefly explained as follows.

During the growth of a two-phase solid from a ternary melt, two components of the alloy combine to bring about a eutectic microstructure in the solid, while the third one (the ''ternary'' component) is rejected into the liquid and generates a Mullins-Sekerka dynamics—i.e., a large-scale cellular instability of the eutectic growth front at V higher than a threshold value V_c [8]. This gives rise to multiscale solidification patterns called eutectic cells at V slightly higher than V_c, and eutectic (or two-phase) dendrites at $V \gg V_c$ [9]. So far eutectic dendrites have only been characterized as elongated objects with a regular internal two-phase microstructure, using *post-mortem* metallographic cross-sectioning [10]. We present a real-time study of the morphology and dynamics of these entities. A thin-sample *sp* dendrite is shown in Fig. 1. As can be seen, *sp* dendrites have a parabolic outer shape (or envelope) in the tip region—which is a defining feature of dendritic solidification [11]—and a helicoidal eutectic microstructure. We establish that this microstructure is generated by a rotating spiral pattern operating at the tip of the entity, hence its name. We show that the spiral mechanism selects both the spacing of the eutectic microstructure and the tip radius of the *sp* dendrite but not its direction of growth.

We used a transparent succinonitrile-(d)camphor (SCN-DC) base pseudo-ternary-eutectic alloy called SCN-DC-NA [12], and studied its directional solidification along the SCN-DC univariant line [13], i.e., under such conditions that the solid is a composite of two crystal phases, namely, a SCN-rich (α) and a DC-rich (β) phase. Previous studies showed that the α-liquid, β-liquid, and $\alpha - \beta$ interfaces all have a weak anisotropy [14]. The material constant K_{JH}, which gives the order of magnitude of the eutectic spacing

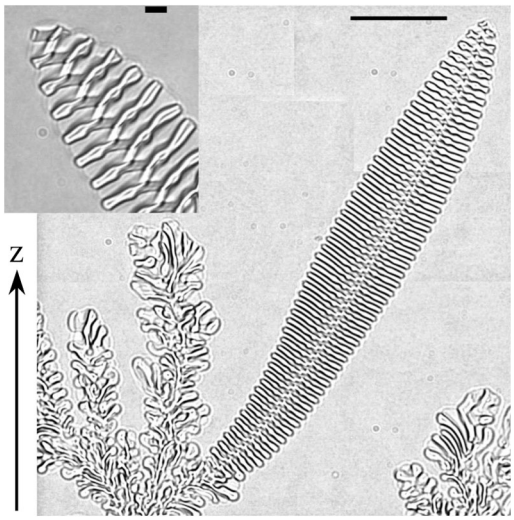

FIG. 1. A *sp* dendrite in process of overgrowing a two-phase branched structure during thin-sample directional solidification of the SCN-DC-NA ternary-eutectic alloy. The interfaces with a strong contrast are those of the DC-rich crystal phase. Bar: 100 μm. **z**: direction of the thermal gradient. Inset: Tip of a steady *sp* dendrite. $V = 0.10\ \mu\mathrm{m\,s^{-1}}$. Bar: 10 μm.

λ via the Jackson-Hunt scaling law $\lambda \sim \sqrt{K_{\mathrm{JH}}} V^{-1/2}$ [5], was measured to be 10.2 $\mu\mathrm{m}^3\,\mathrm{s}^{-1}$ in the binary SCN-DC eutectic, and is likely to remain near this value along the SCN-DC line of SCN-DC-NA. We used flat glass crucibles of internal cross section $w \times 6\ \mathrm{mm}^2$, where w is the sample thickness. Experiments were performed in either bulk ($w = 0.4$ mm) or thin ($w = 0.012$ mm) samples. The samples are placed between a cold oven and a hot oven. A thermal gradient of $7 \pm 1\ \mathrm{K\,mm}^{-1}$ is established by heat diffusion along the sample. The thermal-gradient axis $\mathbf{z}$ is oriented vertically to minimize thermal convection. Solidification is carried out by pulling the sample in the $-\mathbf{z}$ direction. During the pulling, the growth front remains practically immobile in the laboratory reference frame and is observed in real time with an optical microscope. The direction of observation $\mathbf{y}$ is normal to the sample plane. The difference in optical index between phases, which is the only source of optical contrast, is small between α and the liquid, and large between β and the other two phases. Usable images of bulk *sp* dendrites were obtained with a long-distance microscope (Fig. 2). Further details about the experimental methods can be found elsewhere [15].

Because of the high concentration of the ternary component in the alloy, V_c was very low in our system, and the primary cellular bifurcation [16,17] was not observed within the explored V range (0.015–0.71 $\mu\mathrm{m\,s}^{-1}$). After a transient, the growth front acquired an open two-phase branched structure (BS) with a broad (several kelvin wide) "mushy zone" at the rear of a stationary leading edge. Many *sp* dendrites spurting from the two-phase branches were observed. Most were stopped in their incipient stage by collisions (Fig. 3), but some overgrew the BS leading edge, as illustrated in Fig. 1. At long solidification times, a mixed state combining a BS with a few isolated *sp* dendrites was observed [Fig. 2(c)]. We made sure that the *sp* dendrites grew far from the sample walls using focal series [Fig. 2(d)]. The difference in undercooling between the BS leading edge and the tips of the *sp* dendrites was of about 1 K.

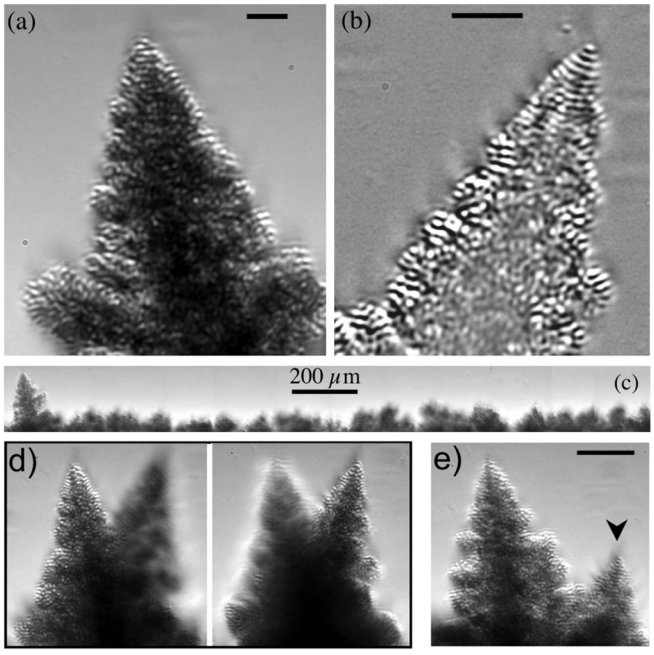

FIG. 2. Bulk *sp* dendrites with different growth rates. (a) 0.28 $\mu\mathrm{m\,s}^{-1}$; (b) 0.95 $\mu\mathrm{m\,s}^{-1}$. Bars: 20 μm. The α lamellae appear black and the β lamellae white. (c) Mixed state. $V = 0.28\ \mu\mathrm{m\ s}^{-1}$. (d) Snapshots from a focal series performed on two *sp* dendrites traveling laterally past each other. The plane of focus was displaced by 120 ± 10 μm between the snapshots. (e) Creation of a new *sp* dendrite (arrow) through side branching. $V = 0.42\ \mu\mathrm{m\,s}^{-1}$. Bars: 20 μm.

Steady *sp* dendrites traveled laterally at an essentially constant velocity. Their actual growth rate was thus $v_s = V/\cos\phi$, where ϕ is their tilt angle with respect to $\mathbf{z}$. The value of ϕ varied from a steady *sp* dendrite to another at fixed V. The tilt angle of some *sp* dendrites was observed to vary slowly over time in response to an external perturbation such as a V jump. *Sp* dendrites traveling in opposite directions passed each other unaltered [Fig. 2(d)], indicating that the range of interaction between *sp* dendrites was short (< 100 μm). The range covered by the steady-state values of ϕ was $-25°$ to $25°$. To sum up, the observed *sp* dendrites were solitary entities with a broad directional degeneracy. Figure 2(e) shows a mother and a daughter *sp* dendrite, almost certainly composed of the same α and β crystals, with largely different tilt angles, demonstrating that ϕ was insensitive to crystallographic factors. This is not surprising knowing the weak interfacial anisotropy of the alloy under study, but suggests that the nondirectional solitary character of the *sp* dendrites in this alloy might be linked to its weak interfacial anisotropy.

In thin samples, the existence of a rotating spiral pattern at the tip of the *sp* dendrites is demonstrated by the alternate bright and dark optical contrast of the successive lamellae of the β phase [Fig. 1 (inset)], and, more directly, by top views of spiral cores inside the mushy zone (Fig. 3). Both right- and left-handed spirals were observed, proving that the chirality of the DC molecules did not come into play. In bulk samples, evidence of the regular rotation of the spiral pattern was provided by spatiotemporal diagrams (Fig. 4). The period of rotation τ_s of the spirals was measured by this method. Spatiotemporal diagrams from

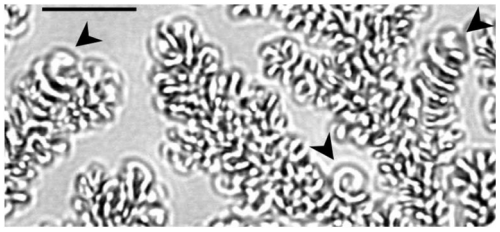

FIG. 3. Incipient *sp* dendrites (arrows) imprisoned in the mushy zone of the branched structure. Thin sample. Bar: 20 μm.

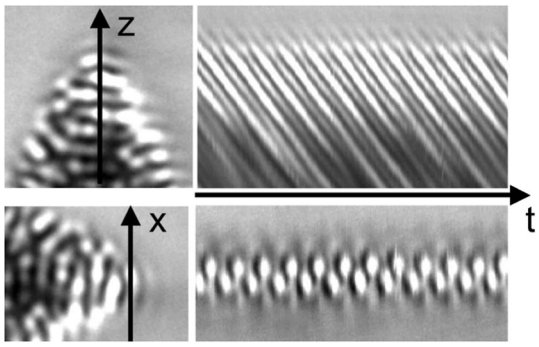

FIG. 4. Left: Tip of a bulk *sp* dendrite. **z** and **x**: lines along which grey level distributions were recorded. Right: spatiotemporal diagrams. *t*: time. Arbitrary space and time scales.

thin *sp* dendrites were similar to those from bulk ones, showing that the spiral mechanism was not altered by confinement effects.

The tip radius ρ_s of the *sp* dendrites as well as the extension of their tip region were determined by fitting parabolas through the experimentally observed profiles. The extension of the tip region ranged from about 5 to $10\rho_s$. These morphological features conform to the theory of diffusive dendrites [11]. The side branching process of *sp* dendrites is characterized by strong interactions of the deformed envelope with the underlying eutectic pattern. The disruption of the spiral pattern caused by side branching is clearly visible in Fig. 2. The feedback effect of this disruption on the development of the side branches is less obvious. However, it is clear that the formation of a spiral embryo from the perturbed eutectic pattern is a necessary stage in the development of new independent *sp* dendrites. Such events were occasionally observed during this study [Fig. 2(e)].

Figure 5 shows an elementary geometrical model of *sp* dendrites which combines two simplifying assumptions, namely, that the envelope forms a paraboloid of revolution, and that the trajectories of the basic eutectic entities are orthogonal to the envelope (normal-growth model [18]). In cylindrical coordinates (r, θ, z) and ρ_s units, the equation for the envelope reads $z = -r^2/2$. The interphase boundaries form two interlaced helicoidal surfaces of equations

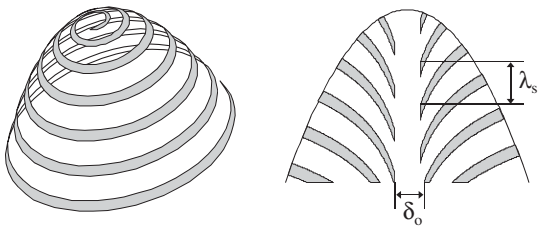

FIG. 5. Normal-growth model of the tip of a *sp* dendrite. $\lambda_s = \rho_s$, $\delta_o = 0.6\rho_s$, $\eta = 0.3$. One of the eutectic phases is shaded grey. Left: 3D view of the surface. Right: Longitudinal cross section.

$z = \ln r - \lambda_s(\theta - \theta_o)/2\pi$, where λ_s is the helix step (or, equivalently, the eutectic spacing far from the tip) and θ_o is a constant, which can be taken to be zero for the $\alpha - \beta$ boundary and $2\pi\eta$ for the $\beta - \alpha$ boundary, where η is the phase fraction of β in the solid far from the tip. This model brings out several interesting features of *sp* dendrites. The key point is that the spiraling motion of the eutectic pattern permits a continuous growth of the *sp* dendrite, for it eliminates the destabilizing processes (such as the creation or termination of a eutectic basic entity) that occur in other types of two-phase fingers [16]. Further features of the *sp* dendrites are a central single-phase (in our case, α) fiber, and the 2D alternate patterns (lamellar arrays shifted by $\lambda_s/2$ on either side of a central fiber) appearing in longitudinal cross sections. This last feature, which can be seen clearly in Fig. 1, can be used to identify *sp* dendrites from sections of opaque ternary alloys. The only obvious discrepancy between the model and the experimental observations concerns the shape of the eutectic lamellae near the central fiber. Clearly, the cores of the spirals expand much more rapidly in reality than in the model.

Measured values of $\lambda_s = v_s\tau_s$ and ρ_s are plotted as a function of v_s in Fig. 6. Despite a relatively large experimental scatter, it is clear that both quantities are decreasing functions of v_s. Furthermore, λ_s is close to the Jackson-Hunt scaling length $\lambda_{JH} = \sqrt{K_{JH}}v^{-1/2}$ for the alloy under study, as could be expected from recent studies of the stability of 3D eutectic patterns [19–21]. More remarkably, ρ_s also is close to λ_{JH}, which means that $\rho_s^2 v_s$ is a constant ($\approx 5.7\ \mu m^3\ s^{-1}$) within experimental accuracy, and that ρ_s is close to λ_s ($\rho_s/\lambda_s \approx 0.79$). Thus, like standard dendrites, *sp* dendrites obey a $\rho^2 v = \text{const}$ scaling law. In all likelihood, this scaling law is imposed to the *sp* dendrites via the condition that ρ_s must be close to λ_s,

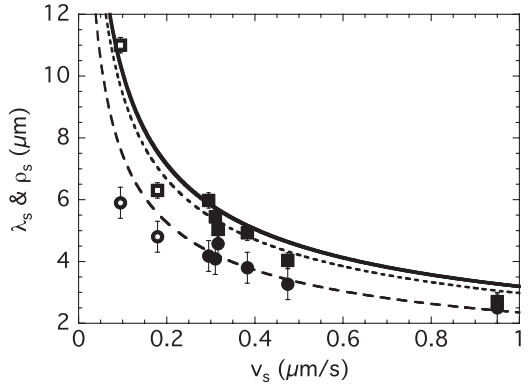

FIG. 6. Measured values of the spiral step λ_s (squares) and tip radius ρ_s (disks) of *sp* dendrites as a function of their growth velocity v_s. Filled (open) symbols: bulk (thin) samples. Thick line: Jackson-Hunt scaling length λ_{JH} for the binary SCN-DC eutectic [14]. Broken and dotted lines: best $v_s^{-1/2}$ fits through the bulk-sample data points for λ_s and ρ_s, respectively. The best fits correspond to $\lambda_s/\lambda_{JH} = 0.94$ and $\rho_s/\lambda_{JH} = 0.75$, respectively.

this last quantity being itself subjected to a $\lambda_s^2 v = \text{const}$ scaling law by stability conditions pertaining to the eutectic patterns. If this is correct, the phenomenon that remains to be explained is the $\rho_s \approx \lambda_s$ relationship. On this point, we are reduced to conjectures for lack of knowledge of the dynamics of eutectic spiral patterns. Planar eutectic spirals have been observed in a few faceted eutectics [22,23], but the *curved* eutectic spirals observed in this study are the first instance of nonfaceted eutectic spirals ever noted, to our knowledge. On the other hand, spiral patterns (or waves) are a common occurrence in chemical, biological and hydrodynamical nonlinear systems [24,25], including *curved* reaction or diffusion systems [26]. It is interesting to note that, in the last-named systems, spiral waves are attracted by the points of highest Gaussian curvature of the system, and that their rotation period is a monotonic function of this curvature. The same seems to be true of the curved eutectic spirals observed during this study.

The dynamics of *sp* dendrites, as defined above, involves no specific property of the ternary-eutectic alloy under study, except perhaps the weak anisotropy of its interfaces. Thus, *sp* dendrites are likely to be a widespread growth shape of weakly anisotropic ternary eutectics. In support to this conclusion, we note that two-phase dendrites exhibiting the characteristic alternate lamellar pattern of longitudinally sectioned *sp* dendrites can be found in the literature about metallic ternary-eutectic alloys. Interestingly, this is true of some ternary eutectics with a strong interfacial anisotropy. In this case, however, *sp* dendrites seem to form dense directional arrays [27], contrary to what was observed during this study. This suggests that a strong interfacial anisotropy does not prevent the existence of *sp* dendrites, but suppresses their directional degeneracy.

We thank V. T. Witusiewicz, L. Sturz, and S. Rex from ACCESS (Aachen, Germany) for providing the alloy and helping in the preparation of the samples. This work was supported by the Centre National d'Etudes Spatiales, France.

*akamatsu@insp.jussieu.fr

[1] M. Asta, C. Beckermann, A. Karma, W. Kurz, R. Napolitano, M. Plapp, G. Purdy, M. Rappaz, and R. Trivedi, Acta Mater. **57**, 941 (2009).
[2] M. Cross and P. Hohenberg, Rev. Mod. Phys. **65**, 851 (1993).
[3] V. G. Smith, W. A. Tiller, and J. W. Rutter, Can. J. Phys. **33**, 723 (1955).
[4] K. Somboonsuk, J. T. Mason, and R. Trivedi, Metall. Trans. A **15**, 967 (1984).
[5] K. A. Jackson and J. D. Hunt, Trans. Metall. Soc. AIME **236**, 1129 (1966).
[6] U. Hecht, L. Granasy, T. Pusztai, B. Böttger, M. Apel, V. Witusiewicz, L. Ratke, J. De Wilde, L. Froyen, D. Camel, B. Drevet, G. Faivre, S. G. Fries, B. Legendre, and S. Rex, Mater. Sci. Eng. **46**, 1 (2004).
[7] *Phase Transformations in Multicomponent Melts*, edited by D. M. Herlach (Wiley-VCH, Weinheim, 2008).
[8] W. W. Mullins and R. F. Sekerka, J. Appl. Phys. **35**, 444 (1964).
[9] W. Kurz and D. J. Fisher, *Fundamentals of Solidification* (Trans Tech Publications, Zurich, Switzerland, 1998).
[10] M. D. Rinaldi, R. M. Sharp, and M. C. Flemings, Metall. Trans. **3**, 3139 (1972).
[11] Y. Pomeau and M. Ben Amar, in *Solids Far From Equilibrium*, edited by C. Godrèche (Cambridge University Press, Cambridge, England, 1992), p. 365.
[12] L. Sturz, V. T. Witusiewicz, U. Hecht, and S. Rex, J. Cryst. Growth **270**, 273 (2004). The alloy composition is (in wgt %) 34succinonitrile-44(d)camphor-19neopentylglycol-3aminomethylpropanediol and corresponds to an invariant point at 53 K. This alloy is ''pseudo ternary'', which means that the combined effects of neopentylglycol and aminomethylpropanediol are practically the same as those of a single component (designated as NA) under the conditions of our experiments.
[13] In directional solidification, the variance (the number of components of the alloy minus the number of solid phases in coexistence with the liquid) represents the number of degrees of freedom available to change the temperature of the solid-liquid interface, and thus deform it in the direction of the thermal gradient.
[14] S. Akamatsu, S. Bottin-Rousseau, M. Perrut, G. Faivre, L. Sturz, and V. Witusiewicz, J. Cryst. Growth **299**, 418 (2007).
[15] S. Bottin-Rousseau, M. Perrut, C. Picard, S. Akamatsu, and G. Faivre, J. Cryst. Growth **306**, 465 (2007).
[16] S. Akamatsu and G. Faivre, Phys. Rev. E **61**, 3757 (2000).
[17] M. Plapp and A. Karma, Phys. Rev. E **60**, 6865 (1999); Phys. Rev. E **66**, 061608 (2002).
[18] W. Datye and J. S. Langer, Phys. Rev. B **24**, 4155 (1981).
[19] S. Akamatsu, S. Bottin-Rousseau, and G. Faivre, Phys. Rev. Lett. **93**, 175701 (2004)
[20] M. Perrut, S. Akamatsu, S. Bottin-Rousseau, and G. Faivre, Phys. Rev. E **79**, 032602 (2009).
[21] A. Parisi and M. Plapp, Acta Mater. **56**, 1348 (2008).
[22] R. L. Fullman and L. Wood, Acta Metall. **2**, 188 (1954).
[23] J. D. Hunt and K. A. Jackson, Trans. Metall. Soc. AIME **236**, 843 (1966).
[24] B. Vasiev, F. Siegert, and C. Weijer, Phys. Rev. Lett. **78**, 2489 (1997), and references therein.
[25] M. Cross, Physica (Amsterdam) **97D**, 65 (1996), and references therein.
[26] N. Manz, V. A. Davydov, S. C. Müller, and M. Bär, Phys. Lett. A **316**, 311 (2003).
[27] S. A. Souza, C. T. Rios, A. A. Coelho, P. L. Ferrandini, S. Gama, and R. Caram, J. Alloys Compd. **402**, 156 (2005). A section through a regular array of (presumably spiral) two-phase dendrites in the (in at %) 49.3Fe-39.7Cr-11Nb eutectic alloy is shown in the Fig. 6 of this reference.